Journal of Inorganic Biochemistry 202 (2020) 110817

Contents lists available at ScienceDirect

Journal of Inorganic Biochemistry

journal homepage: www.elsevier.com/locate/jinorgbio

# Crystal structure, DNA crosslinking and photo-induced cytotoxicity of oxovanadium(IV) conjugates of boron-dipyrromethene

Arun Kumar[a], Akanksha Dixit[b], Somarupa Sahoo[a], Samya Banerjee[a], Arnab Bhattacharyya[a], Aditya Garai[a], Anjali A. Karande[b,*], Akhil R. Chakravarty[a,*]

[a] Department of Inorganic and Physical Chemistry, Indian Institute of Science, Sir C.V. Raman Avenue, Bangalore 560012, India
[b] Department of Biochemistry, Indian Institute of Science, Sir C.V. Raman Avenue, Bangalore 560012, India

ARTICLE INFO

*Keywords:*
Vanadium
Bioinorganic chemistry
DNA crosslink
Photodynamic therapy
Crystal structure

ABSTRACT

Cis-dichloro-oxovanadium(IV) complexes $[VO(L^1/L^2)Cl_2]$, where $L^1$ is N-(4-(5,5-difluoro-1,3,7,9-tetramethyl-5H-4$\Lambda^4$,5$\Lambda^4$-dipyrrolo[1,2-c:2′,1′-f][1,3,2]diazaborinin-10-yl)benzyl)-1-(pyridin-2-yl)-N-(pyridin-2-ylmethyl) methanamine in **1** and $L^2$ is N-(4-(5,5-difluoro-2,8-diiodo-1,3,7,9-tetramethyl-5H-4$\Lambda^4$,5$\Lambda^4$-dipyrrolo[1,2-c:2′,1′-f][1,3,2]diazaborinin-10-yl)benzyl)-1-(pyridin-2-yl)-N-(pyridin-2-ylmethyl)methanamine in **2**) having 4,4-difluoro-4-bora-3a,4a-diaza-s-indacene as boron-dipyrromethene (BODIPY) appended dipicolylamine bases were prepared, characterized and their photocytotoxicity studied. X-ray crystal structure of **1** showed distorted octahedral geometry with a $V^{IV}ON_3Cl_2$ core having Cl-V-Cl angle of 91.93(4)°. The complexes showed variable solution conductivity properties. They were non-electrolytes in dry DMF at 25 °C but showed 1:1 electrolytic behavior in an aqueous medium due to dissociation of one chloride ligand as evidenced from the mass spectral study. Complexes **1** and **2** showed absorption bands at 500 and 535 nm, respectively. The calf thymus DNA melting study revealed their interaction through DNA crosslinking on exposure to light which was further confirmed from the alkaline agarose gel electrophoresis using plasmid supercoiled pUC19 DNA. Complex **2** showed disruption of the mitochondrial membrane potential in the JC-1 (1,1′,3,3′-tetraethyl-5,5′,6,6′-tetrachloroimidacarbocyanine iodide) assay. The complexes were photocytotoxic in visible light (400–700 nm, power: 10 J cm$^{-2}$) in cervical cancer HeLa and breast cancer MCF-7 cells. Complex **2** having a photoactive diiodo-boron-dipyrromethene moiety gave a singlet oxygen quantum yield ($\Phi_\Delta$) value of ~0.6. It showed singlet oxygen mediated apoptotic photodynamic therapy activity with remarkably low $IC_{50}$ (half maximal inhibitory concentration) value of ~0.15 μM. The cis-disposition of chlorides gave a cis-divacant 4-coordinate intermediate structure from the density functional theory (DFT) study thus mimicking the DNA crosslinking property of cisplatin.

## 1. Introduction

Targeted chemotherapy has emerged as a new therapeutic modality in cancer management and cure [1–10]. This methodology primarily relies on inducing stress signals for causing DNA damage [11]. Also, in the traditional treatment of cancer using cisplatin (CP) and its analogues, the drug targets nuclear DNA via crosslinking [12]. However, these platinum-based chemotherapeutic drugs suffer from drawbacks which include multiple drug resistance arising from the poor selectivity of the drug towards differentiating between normal and cancerous cells [13–16]. One of the major inadequacies of CP is the administration of the drug in its active form from rapid dissociation of two chlorides. To avoid the drawbacks associated with the available metal based chemotherapeutics, several prodrug candidates involving various transition metals have been developed, which are designed for cancer cell selectivity either chemically or by photochemical means [17–22]. In the therapeutic regime, considering first row transition elements, vanadium metal is of importance with its ability to suppress the chemically induced tumorigenesis [23]. Also, decavanadate, known to behave as insulin mimic, is reported to possess antitumor activity [24]. In the chemistry of platinum-based chemotherapeutics, Lippard et al. have reported dormant platinum(IV) prodrugs which attain activity upon cellular reduction of the metal to generate the active platinum(II) species [15]. Sadler et al. have reported organometallic iridium(III) half-sandwich cyclopentadienyl complexes showing significant anticancer activity [22]. Light mediated cancer treatment provides useful

* Corresponding authors.
*E-mail addresses:* anjali@iisc.ac.in (A.A. Karande), arc@iisc.ac.in (A.R. Chakravarty).

https://doi.org/10.1016/j.jinorgbio.2019.110817
Received 29 July 2019; Received in revised form 27 August 2019; Accepted 1 September 2019
Available online 05 September 2019
0162-0134/ 

methodology which dates back to psoralens that get activated by UV-A light as an activator [25]. In the chemistry of photo-chemotherapeutics, Photofrin® as a haematoporphyrin derivative is currently used as photodynamic therapy (PDT) drug displaying its activity in red light (633 nm) generating singlet oxygen as the reactive oxygen species (ROS) in a type-II pathway [26–28]. Photo-activated chemotherapy (PACT), recently developed by Sadler and co-workers, utilizes light as a mediator to specifically activate the chemotherapeutics in cancer cells leaving the photo unexposed healthy cells unaffected [29,30]. In PACT, inactive pseudo-octahedral platinum(IV) complexes get activated by UV-A or blue light to generate active platinum(II) species akin to cisplatin in the cancer cells. Current efforts are on to use low-energy visible light for activation of the metal-based anticancer agents due to better tissue penetration of low energy visible light than the UV-A light [31–35].

The work presented here originates from our efforts to tailor vanadium(IV) complexes with an ability to act simultaneously as a transcription inhibitor like cisplatin and a PDT agent like Photofrin® [36,37]. Vanadium, being an essential bio-element and vanadate being known to induce cell death via mitochondrial membrane disruption, is chosen for our study to design complexes showing dual activity, namely, chemotherapeutic action from DNA crosslinking and photo-induced cytotoxicity on visible light irradiation [38]. We have recently reported an oxovanadium(IV) complex of formulation $[VO(L^1)Cl_2]$ (**1**) with NNN-donor tridentate base ($L^1$) having a pendant BODIPY (boron-dipyrromethene) moiety ($L^1$ = N-(4-(5,5-difluoro-1,3,7,9-tetramethyl-5H-4ʌ$^4$,5ʌ$^4$-dipyrrolo[1,2-c:2′,1′-f][1,3,2]diazaborinin-10-yl)benzyl)-1-(pyridin-2-yl)-N-(pyridin-2-ylmethyl)methanamine) [39]. The complex being fluorescent showed only moderate photocytotoxicity towards cancer cells and the study was primarily centered on cellular imaging. Herein, we report the synthesis, characterization and singlet oxygen mediated photo-induced anticancer activity of a new BODIPY-appended cis-dichloro oxovanadium(IV) complex of formulation $[VO(L^2)Cl_2]$ (**2**), where $L^2$, N-(4-(5,5-difluoro-2,8-diiodo-1,3,7,9-tetramethyl-5H-4ʌ$^4$,5ʌ$^4$-dipyrrolo[1,2-c:2′,1′-f][1,3,2]diazaborinin-10-yl)benzyl)-1-(pyridin-2-yl)-N-(pyridin-2-ylmethyl)methanamine, having a pendant diiodinated boron-dipyrromethene moiety has the ability to generate singlet oxygen as the reactive oxygen species (ROS) thus making the complex potentially suitable for photo-chemotherapeutic applications (Fig. 1). Structure of complex **1** having a BODIPY ligand without iodide atoms is elucidated from single crystal X-ray diffraction study. Significant results of this work include: (i) X-ray structural characterization of the BODIPY complex **1**, (ii) DNA crosslinking property observed in visible light (400–700 nm) by the complexes, (iii) Mitochondrial membrane disruption by complex **2** from JC-1 (1,1′,3,3′-tetraethyl-5,5′,6,6′-tetrachloroimidacarbocyanine iodide) dye assay, (iv) singlet oxygen mediated PDT activity of complex **2** in visible light (400–700 nm) giving $IC_{50}$ (half maximal inhibitory concentration) values in sub-micromolar concentration in the cancer cells with relatively low dark toxicity, and (v) rationalization of the cisplatin mimicking properties from density functional theory (DFT) studies giving a cis-divacant structure of the intermediate species on loss of two chloride ligands on photo-exposure. Complex **2** exemplifies a rare dual action chemo-and photo-chemotherapeutic agent.

## 2. Experimental

### 2.1. Materials

All materials were procured from commercial sources (s.d. Fine Chemicals, India; Sigma-Aldrich, USA) and were used as such. The solvents were dried following literature protocols [40]. 3-(4,5-Dimethylthiazol-2-yl)-2,5-diphenyltetrazolium bromide (MTT), Dulbecco's modified eagles medium (DMEM), Dulbecco's phosphate buffered saline (DPBS), ethidium bromide (EB) and agarose (molecular biology grade), Annexin-V/PI, calf thymus (ct) DNA, DCFDA (2′,7′-dichlorofluorescin diacetate) and JC-1 (1,1′,3,3′-tetraethyl-5,5′,6,6′-tetrachloroimidacarbocyanine iodide) dye were procured from Sigma-Aldrich, USA. Supercoiled (SC) pUC19 DNA (caesium chloride purified) was purchased from Bangalore Genei (India). Fetal bovine serum (FBS) was procured from Gibco®. The ligands, namely, $L^1$ = N-(4-(5,5-difluoro-1,3,7,9-tetramethyl-5H-4ʌ$^4$,5ʌ$^4$-dipyrrolo[1,2-c:2′,1′-f][1,3,2]diazaborinin-10-yl)benzyl)-1-(pyridin-2-yl)-N-(pyridin-2-ylmethyl)methanamine for **1** and $L^2$ = N-(4-(5,5-difluoro-2,8-diiodo-1,3,7,9-tetramethyl-5H-4ʌ$^4$,5ʌ$^4$-dipyrrolo[1,2-c:2′,1′-f][1,3,2]diazaborinin-10-yl)benzyl)-1-(pyridin-2-yl)-N-(pyridin-2-ylmethyl)methanamine for **2** were prepared following literature reports [41].

### 2.2. Instrumentation

The fluorescence, electronic and infrared spectra were recorded using Perkin-Elmer LS55, Perkin-Elmer Spectrum 650 and Bruker Alpha spectrophotometer respectively. Molar conductivity measurement was made with a Control Dynamics (India) conductivity meter standardized with 0.01 M KCl solution at room temperature. Electrochemical measurements were made at 298 K using EG&G PAR model 253 Versastat potentiostat/galvanostat and a three electrode setup with glassy carbon working, platinum wire auxiliary and saturated calomel reference electrode (SCE). Tetrabutylammonium perchlorate (TBAP, 0.1 M) in DMF was used as a supporting electrolyte. Magnetic susceptibility of the complexes was measured using Sherwood scientific magnetic susceptibility balance at 298 K. Electrospray ionization mass spectra (ESI-mass) were recorded using Agilent 6538 Ultra high definition (UHD) accurate Mass-Q-TOF (LC-HRMS) instrument. Fluorescence assisted cell sorting experiments were done using FACS Verse instrument (BD Biosciences).

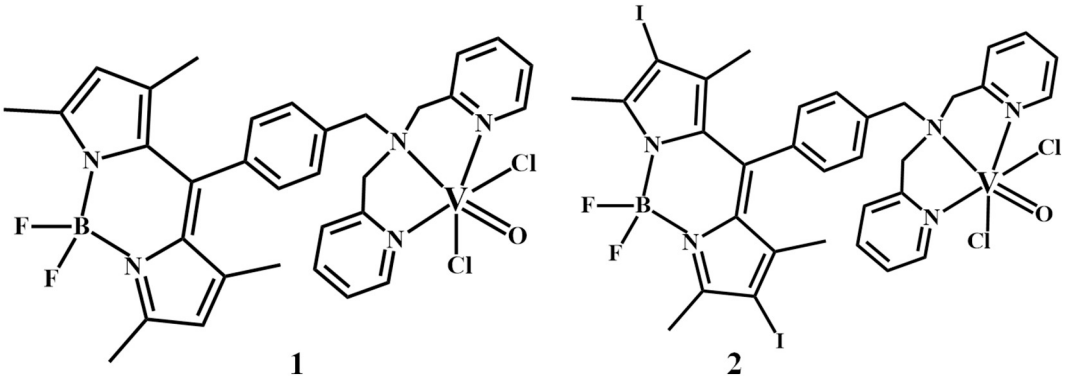


**Fig. 1.** Cis-dichloro-oxovanadium(IV) complexes (**1**, **2**) having ligands $L^1$ = N-(4-(5,5-difluoro-1,3,7,9-tetramethyl-5H-4ʌ$^4$,5ʌ$^4$-dipyrrolo[1,2-c:2′,1′-f][1,3,2]diazaborinin-10-yl)benzyl)-1-(pyridin-2-yl)-N-(pyridin-2-ylmethyl)methanamine in **1** and $L^2$ = N-(4-(5,5-difluoro-2,8-diiodo-1,3,7,9-tetramethyl-5H-4ʌ$^4$,5ʌ$^4$-dipyrrolo[1,2-c:2′,1′-f][1,3,2]diazaborinin-10-yl)benzyl)-1-(pyridin-2-yl)-N-(pyridin-2-ylmethyl)methanamine in **2**.

### 2.3. Synthesis of $[VO(L^1/L^2)Cl_2]$ (1, 2)

Complex **1** having ligand $L^1$ was prepared following our reported procedure and the purity of the complex was ascertained from satisfactory elemental analysis data [39]. Complex **2** was synthesised by initially dissolving vanadium(III) chloride (0.1 g, 0.6 mmol) in 10 mL methanol and stirring in air for 30 min till the solution turned to green during this period [39]. The green solution was purged with nitrogen and a methanol solution of the ligand $L^2$ (0.5 g, 0.6 mmol) was added drop-wise to this mixture. The complex got precipitated after 1 h. The solid was filtered and washed with cold ethanol and dried in vacuum over $P_4O_{10}$ (isolated yield: 0.45 g, ~80%).

Anal. Calcd for $C_{32}H_{32}BCl_2F_2N_5OV$ (**1**) (MW: 673.2903): C, 57.08; H, 4.79; N, 10.40. Found: C, 57.20; H, 4.90; N, 10.30. Anal. Calcd for $C_{32}H_{30}BCl_2F_2I_2N_5OV$ (**2**) (MW: 940.1123): C, 41.55; H, 3.27; N, 7.57. Found: C, 41.37; H, 3.51; N, 7.43. ESI-mass in MeOH (*m/z*): 889.0956 $[M - Cl]^+$. UV–Vis in 20% DMSO: DPBS [$\lambda_{max}$/nm ($\varepsilon$/ $M^{-1}$ $cm^{-1}$)]: 780 (60), 535 (36000). FT-IR ($cm^{-1}$): 2128 m, 2000 m, 1598 s, 1545 m, 1437 m, 1294 m, 962 s, 765 w, 675 w, 514 s (s, strong; m, medium; w, weak). $\mu_{eff}$ = 1.61 $\mu_B$ at 298 K.

### 2.4. X-ray crystallographic procedure

Complex **1** as the close analogue of **2** was structurally characterized by single crystal X-ray diffraction method. The crystals were grown by vapor diffusion of diethyl ether to a $CH_3OH$ solution of complex **1**. A crystal suitable for data collection was isolated and mounted on a loop with paraffin oil. The geometric and intensity data were obtained at 100 K using an automated Bruker SMART APEX CCD diffractometer equipped with a fine focus 1.75 kW sealed tube Mo-Kα X-ray source (λ = 0.71073 Å) with increasing ω (width of 0.3° frame) at a scan speed of 5 s per frame. Intensity data were collected using ω-2θ scan mode and required corrections were made for Lorentz-polarization effect and for absorption [42]. The structure was solved using Patterson and Fourier techniques and refined by full matrix least squares method using SHELX system of programs [43]. The hydrogen atoms belonging to the complex were refined by using riding mode at isotropic stage. All non-hydrogen atoms were refined using anisotropic thermal parameters. The perspective view of the molecule was obtained by ORTEP (Oak Ridge Thermal Ellipsoid Plot) [44]. Selected crystallographic parameters are: $C_{32}H_{32}BCl_2F_2N_5OV$, Fw/ g $M^{-1}$ = 673.28, space group *P*ī, a = 7.2070(4) Å, b = 14.7882(9) Å, c = 15.5661(9) Å, α = 90.962(2)°, β = 101.550(2)°, γ = 97.956(2)°, V = 1608.08(16) $Å^3$, Z = 2, $\rho_{calcd}$ = 1.390 g $cm^{-3}$, *T* = 273(2) K, reflections collected/unique: 6892/3811, F(000) = 694.0, Goodness-of-fit = 1.052, R($F_o$) [wR ($F_o$)] = 0.0624 [0.1369] for 3811 reflections [$I > 2\sigma(I)$] and 400 parameters; R (all data) [wR (all data)] = 0.1674 [0.1327]. The CCDC deposition number is 1523110.

### 2.5. Computational study

The energy optimized structures of complex **2** and those of two predicted intermediates on loss of one and two chloride ligands in solution phase with or without light activation were obtained by density functional theory (DFT) using Gaussian09 program [45,46]. The optimized geometries were obtained by DFT with B3LYP (Becke, 3-parameter, Lee–Yang–Parr) level of theory and LanL2DZ (Los Alamos National Laboratory 2 Double-Zeta) basis set. The calculated atomic coordinates for the geometries are provided as supporting information.

### 2.6. Singlet oxygen quantum yield measurement

A steady-state method was employed to measure the singlet oxygen quantum yield ($\Phi_\Delta$) using 1,3-diphenylisobenzofuran (DPBF) as the quencher of singlet oxygen along with Rose Bengal (RB) as the reference dye. The light intensity was constant throughout the photo-irradiation time. This was achieved by measuring the output using an Oriel photodiode detection system (model 7072). The experiments were carried out with a light source of 200 W Xenon Lamp (model 3767) on an Oriel optical bench (model 11,200) with a grating monochromator (model 77,250). Quantum yield for singlet oxygen generation in DMSO was determined by monitoring the photo-oxidation of DPBF during the formation of singlet oxygen using an absorption spectrometer. Concentration of the photosensitizer was adjusted with an optical density of 0.02–0.03 at the irradiation wavelength of 530 nm to minimize the possibility of self-quenching. The photo-oxidation of DPBF was monitored with an interval of 20 s. The following equation was used to calculate the singlet oxygen quantum yield of the sensitizer with respect to the reference: $\Phi_\Delta$ (sample) = $\Phi_\Delta$ (ref) ($m_{sample}/m_{ref}$)/($F_{ref}/F_{sample}$), where $\Phi(^1O_2)$ or $\Phi_\Delta$ is the quantum yield of singlet oxygen, m is the slope from a plot of difference in change in optical density of DPBF (at 411 nm) with respect to the irradiation time, and F is the absorption correction factor, which is given by F = $1–10^{-OD}$ (OD at the irradiation wavelength) [47].

### 2.7. DNA melting

DNA melting experiments were performed in phosphate buffer (pH 6.8) using 190 μM calf thymus (ct) DNA and 20 μM complexes by changing the temperature from 40 to 90 °C at a ramp rate of 1 °C. The graph plotting was done using Origin Lab, version 8 [48].

### 2.8. Cellular studies

The visible light-promoted cytotoxicity of complex **2** in HeLa (Henrietta Lacks) cervical and MCF-7 (Michigan Cancer Foundation-7) breast cancer cells was studied by 3-(4,5-dimethylthiazol-2-yl)-2,5-diphenyl tetrazolium bromide (MTT) assay. The experiments were performed using reported procedures that in detail are given as Supporting Information [49]. A broad-band visible light (400–700 nm) using Luzchem Photoreactor (Model LZC-1, Ontario, Canada; light fluence rate: 2.4 mW $cm^{-2}$; light dose: 10 J $cm^{-2}$) was used. The MTT absorbance at 540 nm was measured using a plate reader (Molecular Devices Spectra Max M5). The cytotoxicity of the complexes was measured as the percentage ratio of absorbance of the treated cells to the untreated controls. The $IC_{50}$ values were determined by using nonlinear regression analysis (Graph Pad Prism 6). The intracellular ROS generation by complex **2** was quantified by 2′,7′-dichlorofluorescein diacetate (DCFDA) assay in both light and dark conditions in HeLa cells using reported procedures [49]. The data were acquired on a FACS (fluorescence-activated cell sorting) Verse flow cytometer (Biosciences, USA). In Annexin-V/FITC (fluorescein isothiocyanate) assay, HeLa cells ($0.25 \times 10^6$) were incubated with the complexes **1** (1.5 μM) and **2** (0.3 μM) for 4 h followed by 1 h of photo-exposure in broad band white light of 400–700 nm using Luzchem photoreactor (light dose = 10 J $cm^{-2}$) in DPBS or in darkness. Annexin-V/FITC was added to the cells and incubated for 10 min in the dark. The cells were then washed and propidium iodide (PI) (1 μL) was added. Thereafter, the fluorescence from the cells was observed via FACS Verse flow cytometer using Cyflogic software for analysis of the results.

## 3. Results and discussion

### 3.1. Synthesis and general properties

Oxovanadium(IV) complex **2** was prepared from a reaction of vanadium(III) chloride in methanol with the ligand $L^2$ having a pendant diodo-BODIPY moiety and characterized from various analytical and spectroscopic data (Table 1). Complex **1** having $L^1$ with a non-iodo BODIPY pendant was studied as a control entity [39]. The light-promoted cytotoxic properties of the complexes were studied from different biological assays. Complex **1** of formulation $[VO(L^1)Cl_2]$ was

**Table 1**
Selected physicochemical data and DNA binding parameters.

| Complex | $\lambda_{max}$[a]/nm ($\varepsilon$/$M^{-1}$ $cm^{-1}$) | $\lambda_{em}$[b]/nm ($\lambda_{ex}$/nm) [$\Phi_F$ ($\Phi_\Delta$)][c] | $E_{pc}$/V[d] | $\Lambda_M$[e]/S $m^2$ $mol^{-1}$ | $\mu_{eff}$[f]/$\mu_B$ | $\Delta T_m$[g]/° |
|---|---|---|---|---|---|---|
| 1[h] | 750 (60), 501 (53000), 471 sh (15000) | 510(450) [0.07 (0.14)] | −0.89 | 81 (155) | 1.62 | 1.2 |
| 2 | 780 (60), 535 (36000) | - [−(0.6)][i] | −0.83 | 85 (154) | 1.61 | 0.5 |

[a] Visible band in 20% aqueous DMF.
[b] In 1:1 (*v*/*v*) DMF (dimethylformamide) and phosphate buffer.
[c] λem and λex are the emission and excitation wavelength. For emission quantum yield, fluorescein was used as a standard ($\Phi_F$ = 0.79 in sodium hydroxide solution of 0.1 M). Rose Bengal was used for $\Phi_\Delta$ measurement.
[d] In DMF-0.1 M TBAP, $E_{pc}$ is cathodic peak potential. All data were measured against SCE. Ferrocene was used as a standard. Scan rate = 100 mV $s^{-1}$.
[e] In aq. DMF. The value upon photo-exposure in 20% aqueous DMF is in bracket.
[f] Solid samples for effective magnetic moments (*T* = 298 K).
[g] The ct-DNA melting temperature.
[h] Characterization data are from reference [39].
[i] The complex being poorly emissive, $\Phi_F$ was not calculated for this complex.

structurally characterized from single crystal diffraction study. The complexes were one-electron paramagnetic species with a $\mu_{eff}$ value of ~1.6 μB at 298 K. Their IR spectra displayed V=O stretching band at ~960 $cm^{-1}$ [50]. The prominent peak in the ESI-mass spectra of the complexes in methanol was assigned to $[M\text{-}Cl]^+$ indicating facile dissociation of one chloride ligand from the dichloro-oxovanadium(IV) complexes in methanol solvent.

The $3d^1$-$VO^{2+}$ complexes displayed a weak vanadium-centred d-d band near 780 nm in 20% aqueous dimethylformamide (DMF). The complexes showed an intense band near 500 nm which is assignable to the BODIPY ligand (Fig. 2) [41]. Complex **2** having the diiodinated-BODIPY ligand is non-emissive due to the presence of two heavy iodine atoms thus making the intersystem crossing (ISC) a facile process to generate singlet oxygen species following a type-II pathway [51]. The complexes showed variable solution conductivity properties (Fig. 2). They were non-electrolytes in dry DMF at 25 °C. The $\Lambda_M$ value increased to ~90 S $m^2$ $mol^{-1}$ in 20% aqueous DMF, indicating 1:1 electrolytic behaviour in an aqueous medium due to dissociation of one chloride ligand with a possibility of generation of a 5-coordinate species in solution as evidenced from the mass spectral study. The value increased marginally to ~100 S $m^2$ $mol^{-1}$ when the solution was kept for a longer duration of 48 h in the dark. A further increase to ~150 S $m^2$ $mol^{-1}$ was observed upon visible light (400–700 nm) exposure of the solutions for 1 h, suggesting the dissociation of the second chloride ligand (Fig. 1). The $\Lambda_M$ value decreased to ~130 S $m^2$ $mol^{-1}$ when the photo-irradiated solution was kept in dark for 24 h, indicating some regeneration of the 1:1 mono-chloro adduct species, possibly at the cis-position of the $VO^{2+}$ moiety. As observed earlier for complex **1**, complex **2** also displayed an irreversible V(IV)-V(III) cyclic voltammetric redox process near −0.9 V (vs. saturated calomel electrode, S.C.E.) in 20% aqueous DMF-0.1 M TBAP (tetrabutylammonium perchlorate) as a supporting electrolyte [39]. The introduction of iodide to the BODIPY core did not show any significant effect on the redox properties of the complexes which is solely dependent on the oxovanadium(IV) moiety in the $VON_3Cl_2$ core. The redox inactivity of the complex within the biological potential window indicated the possibility of no dark cytotoxicity in the presence of cellular thiols. The complexes did not show any V(V)-V(IV) redox process thus suggesting redox stability of the oxovanadium(IV) unit.

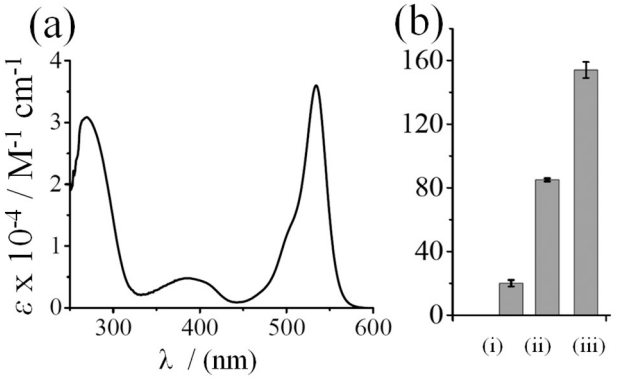


**Fig. 2.** (a) Absorption spectrum of complex **2** in 20% aqueous DMF. (b) Molar conductivity of complex **2** in the unit of S $m^2$ $mol^{-1}$ (y-axis) in (i) dry DMF, (ii) 20% aqueous DMF in the dark and (iii) 20% aqueous DMF after exposure to light (400–700 nm) for 1 h.

### 3.2. Crystal structure

Complex **1** of formulation $[VO(L^1)Cl_2]$ having a BODIPY moiety was crystallized by vapor diffusion of diethyl ether to the methanol solution of the complex and structurally characterized by single crystal X-ray diffraction method. The complex crystallized in the triclinic space group *P*ī with two molecules in the unit cell (Z = 2). An ORTEP view of the complex is shown in Fig. 3. The complex has a distorted octahedral geometry with a $VON_3Cl_2$ core. The NNN-donor ligand displays tridentate chelating mode of bonding in a facial manner. The V(1)-O(1) bond distance is 1.593(2) Å with a bond order of 2.0. The V(1)-Cl(1) and V(1)-Cl(2) bond distances in **1** of ~2.33 Å indicated that these bonds are susceptible to ligand dissociation in an aqueous medium with a possibility of structural change. The V(1)-N(7) bond distance is 2.383(2), which is marginally longer than the V(1)-N(1) and V(1)-N(5) distances due to trans directing influence of the $\{V=O\}^{2+}$ moiety. The

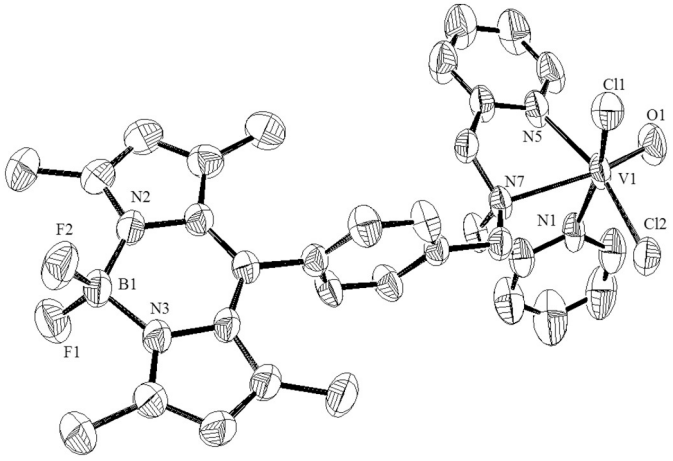


**Fig. 3.** ORTEP view of complex **1** showing atom labelling for vanadium and the heteroatoms. Hydrogen atoms are omitted for clarity. The thermal ellipsoids are at 50% probability level.

**Table 2**
Selected bond distances (Å) and angles (°) for $[VO(L^1)Cl_2]$ (**1**) with estimated standard deviations in the parenthesis.

| | | | |
|---|---|---|---|
| V(1)-N(1) | 2.108(3) | Cl(1)-V(1)-Cl(2) | 91.93(4) |
| V(1)-N(5) | 2.154(3) | N(1)-V(1)-Cl(1) | 163.22(8) |
| V(1)-N(7) | 2.383(2) | N(5)-V(1)-Cl(1) | 88.69(9) |
| V(1)-Cl(1) | 2.333(13) | N(1)-V(1)-Cl(2) | 84.04(8) |
| V(1)-Cl(2) | 2.334(11) | N(5)-V(1)-Cl(2) | 164.05(8) |
| V(1)-O(1) | 1.593(2) | N(1)-V(1)-N(7) | 75.24(10) |
| O(1)-V(1)-N(1) | 94.70(14) | N(7)-V(1)-Cl(1) | 88.70(7) |
| O(1)-V(1)-N(5) | 92.65(13) | N(5)-V(1)-N(7) | 71.76(10) |
| O(1)-V(1)-N(7) | 160.99(13) | N(7)-V(1)-Cl(2) | 92.31(7) |
| O(1)-V(1)-Cl(1) | 102.08(12) | N(1)-V(1)-N(5) | 90.79(12) |
| O(1)-V(1)-Cl(2) | 102.79(11) | | |

phenyl ring and the BODIPY core make an angle of ~120° thus reducing the paramagnetic effect of the metal core on the photophysical properties of the BODIPY unit due to lack of any effective conjugation between these units. The Cl(1)-V(1)-Cl(2) angle of 91.93(4)° indicated *cis*-disposition of two chloride ligands akin to that known for cisplatin. Although we do not have any structural evidence of these paramagnetic complexes in solution, the loss of one labile and one photo-labile chloride ligand is expected to generate an active species with lower coordination number(s) which is expected to show DNA crosslinking property similar to that observed for cisplatin and its analogues. Selected bond distances and bond angles are listed in Table 2. With the complex having two possibilities of chlorides in *cis* or *trans* disposition, the crystal structure unequivocally established the cis structure of the complexes thus mimicking the DNA cross-linking property of cisplatin.

### 3.3. Theoretical study

The atomic coordinates obtained from the crystal structure of complex **1** were used to optimize the structure of complex **2** by B3LYP functional and LanL2DZ basis set with the Gaussian09 suites [45,46]. The optimized structure and the HOMO-LUMO levels of complex **2** were determined. The complex showed distorted octahedral geometry around the metal centre in a similar fashion as is observed in the crystal structure of complex **1** (Fig. 4a). The photophysical properties are based on the frontier molecular orbitals (FMO) that are concentrated over the BODIPY core. Considering the importance of the solution structures of the intermediates for their cellular properties and DNA binding abilities, the DFT calculations were further extended for the intermediate 5-coordinate species on loss of one chloride ligand and a 4-coordinate species on loss of two chloride ligands. This optimization was done with DMSO as the solvent environment. The energy minimized structure indicated distorted trigonal bipyramidal (tbp) geometry around the metal centre for the first intermediate showing rapid loss of one chloride from the 6-coordinate structure as observed in the ESI-mass spectra (Fig. 4b). The energy minimized structure for the 4- coordinated species after removing both the chlorides atoms displayed a rare cis-divacant octahedral geometry around the metal center (Fig. 4c). The five-coordinate intermediate could have two possible geometries, viz. trigonal bipyramidal (tbp) or square-pyramidal. The ligand geometry seems to dictate the distorted tbp structure of the first intermediate. The four-coordinate structure can have three possibilities, viz. square-planar, tetrahedral or cis-divacant structure. Interestingly, the DFT study predicts a rare cis-divacant structure which is likely to aid in the DNA cross-links formation in a similar way that is known for cisplatin.

### 3.4. DNA melting and cleavage studies

The DNA melting experiments were carried out to predict any DNA crosslink formation by the complexes. The duplex DNA at its melting temperature unwinds to give single stranded DNA with an increase in the absorbance at 260 nm as the bases separate out from each other [52]. Crosslinking stabilizes the DNA helix resulting in a small change in the melting temperature. The complexes gave $\Delta T_m$ value of ~1 °C on light (400–700 nm) exposure of the samples. The small $\Delta T_m$ value strongly suggests DNA crosslinking ability of the complexes with the loss of two chloride ligands on light exposure, while they act as DNA groove binders/intercalators in the dark in the presence of one metal-bound chloride ligand (Fig. 5a). This observation is remarkable with DNA crosslinking taking place only by light exposure and not in the dark. Cisplatin as a control gave a similar $\Delta T_m$ value. Ethidium bromide (EB) as a known DNA intercalator showed significantly high $\Delta T_m$ value of 25 °C [53]. The possibility of formation of DNA crosslinks was further probed via alkaline agarose gel electrophoresis. Complexes were incubated with plasmid supercoiled (SC) pUC19 DNA in the dark for 1 h with subsequent photo-irradiation for 1 h using a broad band visible light (400–700 nm). The movement of the plasmid was found to be high in the light-irradiated samples as compared to the samples kept in the dark (Fig. 5b). This could possibly be due to the formation of higher order DNA structures upon crosslink formation.

While the DPBF titration experiments showed singlet oxygen as the ROS, the DPBF experiments using Rose Bengal gave the singlet oxygen quantum yield for complex **2**.

### 3.5. Singlet oxygen generation

BODIPY dyes having heavy atoms are well known to provide stable triplet states which subsequently aid in the formation of highly reactive singlet oxygen species [54-56]. The objective of incorporating $L^2$ with a diiodo-BODIPY moiety in the structure is to make the complex dually active as a transcription inhibitor and a PDT agent with high singlet oxygen quantum yield. In contrast, complex **1** having non-iodo BODIPY in $L^1$ being emissive is not suitable as a photosensitizer. The singlet oxygen quantum yield ($\Phi_\Delta$) was determined by absorbance quenching of 1,3-diphenylisobenzofuran (DPBF) using Rose Bengal (RB) as a standard. DPBF forms endoperoxide on reaction with singlet oxygen ($^1O_2$) and this process reduces the absorbance of DPBF at ~415 nm. This property was utilized to investigate the $^1O_2$ generation ability of the complexes. A solution of DPBF was photo-irradiated (400–700 nm) with the diiodo-BODIPY complex **2** and the dye separately using a long pass of 530 nm over a time period of 1–10 s. The singlet oxygen quantum yield value of the non-emissive complex **2** ($\Phi_\Delta$) was found to be ~0.6. A similar experiment performed with the fluorescent non-iodo BODIPY control complex **1** gave a much lower $\Phi_\Delta$ value of only 0.14. The results indicate complex **2** as an excellent photosensitizer generating singlet oxygen as the ROS.

### 3.6. Cellular assays

Visible light-induced antiproliferative property of the complexes was studied in two different cell lines, viz., HeLa (human cervical) and MCF-7 (human breast cancer), by MTT (3-(4,5-dimethylthiazol-2-yl)-2,5-diphenyltetrazolium bromide) assay (Fig. 7a). The cells were treated with various concentrations of the complexes for 4 h incubation in dark at 37 °C. Subsequently, the cells were irradiated with visible light (400–700 nm) for 1 h. Suitable dark controls were examined to estimate their toxicity in dark. The $IC_{50}$ (half maximal inhibitory concentration) values of the complexes are given in Table 3 along with relevant compounds [39,57,58]. Complex **2** showed low dark toxicity ($IC_{50}$ > 50 μM) in both HeLa and MCF-7 cells. In contrast, the complex gave sub-micromolar $IC_{50}$ value (~0.2 μM) when exposed to light for these cells. A significant enhancement in the PDT activity was observed on changing the BODIPY ligand from **1** to diiodo-BODIPY ligand in complex **2**. This is due to excellent singlet oxygen generation ability of complex **2** over the control complex **1**.

Generation of ROS on light exposure initiating cellular apoptosis is an important aspect of photodynamic therapy (PDT) as the ROS leads to cell death. DCFDA (2′,7′-dichlorofluorescein diacetate) assay as a tool

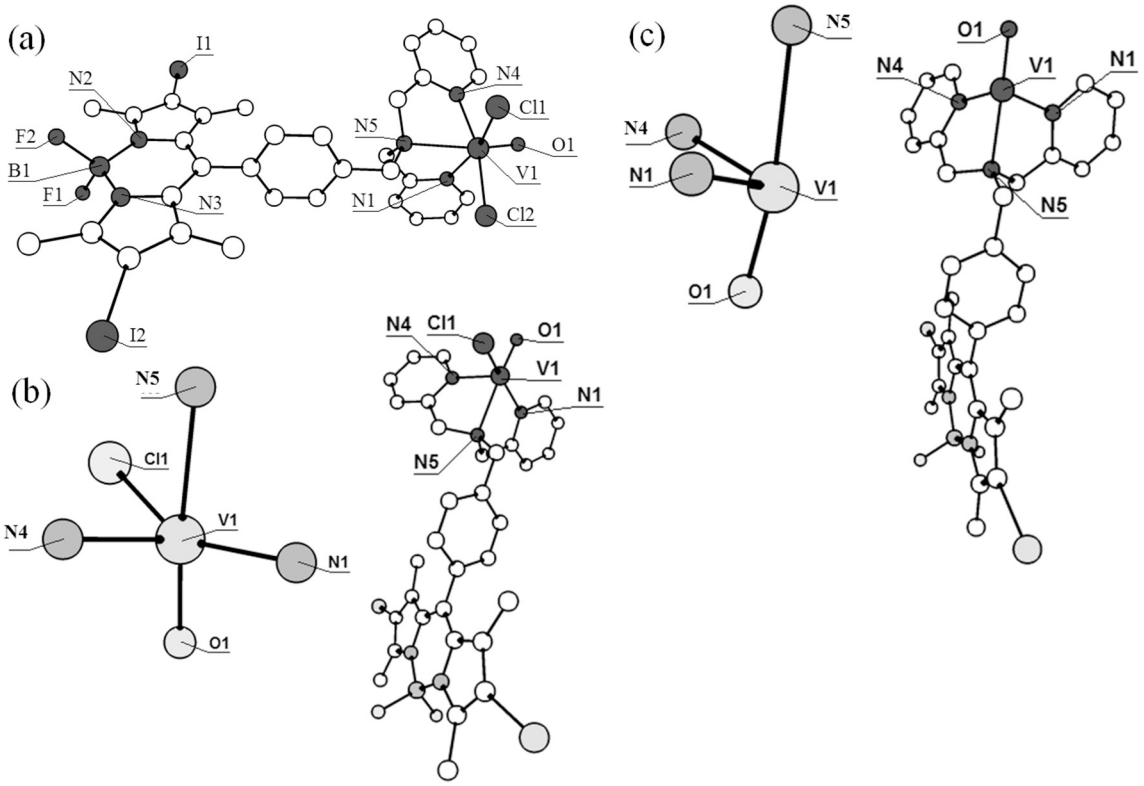


**Fig. 4.** The energy-optimized structures of the diiodo-BODIPY complex **2** (a) along with its two proposed intermediates, viz. (b) and (c) on loss of one and two chloride ligand(s), respectively. The core structures of two intermediate species are also shown. The amine nitrogen atom N(5) of the NNN-donor ligand is located opposite to O(1) of the $VO^{2+}$ moiety in these structures.

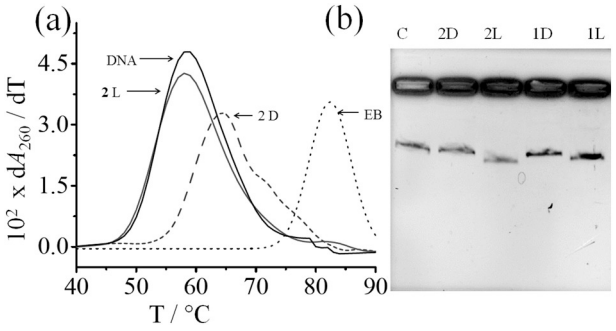


**Fig. 5.** (a) The $\Delta T_m$ plots for ct-DNA (200 μM) treated with complex **2** [D, in dark; L, in light of 400–700 nm] and ethidium bromide (EB in dark) in 5 mM phosphate buffer (pH, 7.2). Complex **2** in dark and light are two different molecular species resulting from loss of one and two chloride ligand(s), respectively. (b) Increase in the movement of circular pUC19 DNA in alkaline agarose gel electrophoresis for complexes **1** and **2** on exposure to light (L), relative to those kept in dark (D) with C as the control.

was used to investigate the generation of ROS by the photosensitizer complex. This assay was performed in HeLa cells using complex **2**. The dye DCFDA which is permeable to live cells gets hydrolysed by intracellular esterase enzyme converting it to DCF, which upon oxidation by ROS becomes fluorescent and emits at 525 nm thus making its detection possible by fluorescence activated flow cytometry [59]. HeLa cells were incubated with complex **2** (0.3 μM) for 4 h in dark at 37 °C. Dark controls were also investigated for comparative study. The mean fluorescence intensity of the oxidized DCF displayed a significant positive shift in the visible light-exposed cells in comparison to the untreated cells or those kept in the dark. This observation unequivocally established generation of cellular ROS by complex **2** only upon light exposure and not in dark (Fig. 6b).

**Table 3**
The $IC_{50}$ values (μM) of complex **2** along with relevant compounds.[a]

| Compound | HeLa | | MCF-7 | |
|---|---|---|---|---|
| | Light[b] | Dark | Light[b] | Dark |
| **2** | 0.15 ( ± 0.02) | > 100 | 0.20 ( ± 0.08) | > 100 |
| Cisplatin[c] | – | 71 ( ± 3) | – | 28 ( ± 3) |
| Photofrin®[d] | 4.3 ( ± 0.2) | > 41 | – | – |

[a] The estimated deviations in the $IC_{50}$ values are given in the parenthesis. The reported $IC_{50}$ values for complex **1** are 1.8 ± 0.6 (Light), > 50 μM (Dark) for HeLa and 3.4 ± 0.4 (Light), > 50 (Dark) μM for MCF-7 cells [39].
[b] The $IC_{50}$ values correspond to 4 h incubation in dark followed by photoexposure for 1 h to visible light of 400–700 nm (10 J $cm^{-2}$).
[c] The $IC_{50}$ values from published report [57].
[d] The $IC_{50}$ values from published report [58].

Annexin-V-FITC/PI (fluorescein isothiocyanate/ propidium iodide) assay was performed on HeLa cells to probe the mechanistic aspects of cell death. The early stages of apoptosis involve flipping of phosphatidylserine from the inner leaflet to the outer leaflet of the cell membrane. Annexin V is a cellular protein that binds to phosphatidylserine, a glycerophospholipid component of the cell membrane. Annexin V, conjugated with a fluorescent dye, can be used to measure the number of apoptotic cells by flow cytometry. Propidium iodide (PI) dye, which is permeable in cells with disrupted cell membrane, was used as a second fluorescent marker to determine the population of cells undergoing necrosis or in late stage of apoptosis. The Annexin-V/PI binding assay was performed with complexes **1** and **2** to explore the mode of cell death in HeLa cells. A 4 h incubation of the cells with **2** (1.5 μM) followed by irradiation with light (400–700 nm, 10 J $cm^{-2}$) showed ~45% of the cells to be Annexin-V and PI positive indicating apoptotic population. The complex did not induce any significant cell death in the dark. Complex **2** (0.3 μM), however, induced ~70% of cells to undergo

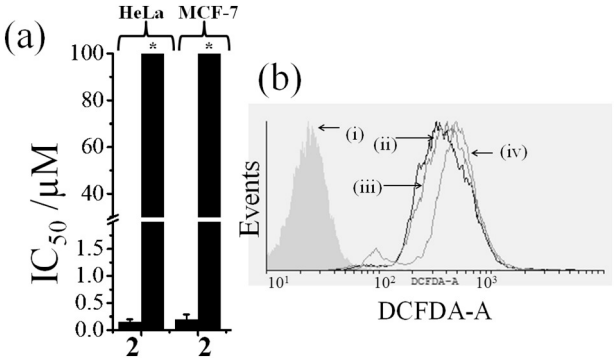


**Fig. 6.** (a) MTT assay data in HeLa and MCF-7 cells on 4 h incubation in dark (right side bar, * indicates 100 μM limiting concentration used) and light (400–700 nm, 10 J $cm^{-2}$) (left side bar). (b) Flow cytometry for ROS generation using DCFDA (2′,7′ –dichlorofluorescin diacetate) assay for complex **2** in HeLa cells. A larger shift implies higher quantity of DCF and ROS generation: (i) cells alone, (ii) cells + DCFDA, (iii) cells + DCFDA + complex (in dark), and (iv) cells + DCFDA + complex (light, 400–700 nm).

apoptosis only upon light exposure (vide supplementary data). The assay suggests that both the complexes remained relatively inactive in the dark but incubation of the cells with the complexes followed by light (400–700 nm) irradiation triggered apoptosis and the effect is significantly more prominent for the diiodo-BODIPY complex **2** than the control complex **1**.

Cellular uptake and localization of the complexes inside the cells are the key factors for the complexes to target various cellular responses [60]. The control complex **1** being fluorescent was used to study the cellular uptake in HeLa and MCF-7 cells after an incubation period of 4 h, using flow cytometry (vide supplementary data). The percentage cell positivity of the complex was monitored. Cells were incubated with varying concentrations of **1** in dark at 37 °C and were monitored for various time periods (1, 2 and 4 h). The complex at 1.5 μM showed almost full uptake in both the cells within 4 h. Mitochondria targeting compounds are of current importance since mitochondria, apart from playing the key role in the intrinsic pathway of apoptosis, is the energy source of the cell. Damage of the mitochondrial DNA in a cell can lead to a dysfunctional organelle resulting in cell death [61]. Our earlier observation showed significant amount of mitochondrial localization of the BODIPY complex **1** in HeLa and MCF-7 cells [39]. Complex **2** was used for the JC-1 (1,1′,3,3′-tetraethyl-5,5′,6,6′-tetrachloroimidacarbocyanine iodide) assay using HeLa and MCF-7 cells. When the mitochondrial potential is high, JC-1 being a potentiometric dye moves inside mitochondria and forms aggregates, while in low mitochondrial potential, the dye remains as monomers. Flow cytometry was used for analysis of the change in mitochondrial membrane potential ($\Delta\Psi_m$) in whole cells. JC-1 dye was excited using an argon laser at a wavelength of 488 nm. Both JC-1 aggregates and monomers exhibited green fluorescence (peak emission at 527 nm) which was quantified in the FL1 channel (530 nm) of the Flow Cytometer. JC-1 aggregates displayed a red spectral shift (peak emission at 590 nm), and was measured in the FL2 channel (585 nm). The HeLa and MCF-7 cells were treated with 0.3 μM of complex **2** for 4 h in dark at 37 °C. Thereafter, the cells were photo-irradiated with visible light (400–700 nm) for 1 h. A significant reduction in the FL2 intensity was observed in the treated cells in comparison to the dark controls (Fig. 7). This could be due to the mitochondrial membrane disruption and this observation was further proved by using valinomycin, a known mitochondrial membrane disrupter, which was used as a positive control.

## 4. Conclusions

BODIPY-appended cis-dichloro-oxovanadium(IV) complexes as cellular imaging and photocytotoxic agents were designed and developed for singlet oxygen-mediated PDT activity and as DNA crosslinking agents. The non-iodo BODIPY complex **1** as control was structurally characterized by X-ray crystallography. The complexes showed DNA crosslinking property due to dissociation of one labile and the other photo-labile chloride ligands. This is evidenced from the DNA melting experiments using the complex in solution kept in dark and on exposure to light. Lay et al. in their recent article on “Stabilities and biological activities of vanadium drugs: What is the nature of the active species?” has shown that the lability of vanadyl(IV) complexes on variation of the physical conditions in the solvents where these species act as pharmaceuticals could lead to decay into naked metal ion and uncomplexed ligand [62]. We have explored this possibility carefully and found that the present complexes are stable in the cellular medium and do not undergo any degradation of the NNN-donor chelating dpa ligands with BODIPY pendants and only the loss of two chloride ligands was observed in our study (vide supporting information, Table S4.). The complex having a diiodo-BODIPY ligand was found to be an excellent photosensitizer showing visible light-induced cellular apoptosis with $IC_{50}$ values in the sub-micromolar concentration range, while being significantly less toxic in dark. The apoptotic pathway involved reactive oxygen species which is solely the singlet oxygen ($^1O_2$). Besides the DNA melting data, the formation of DNA crosslinks on photo-activation was further evidenced from the alkaline agarose gel electrophoresis study. In addition, the BODIPY complexes primarily localized in the

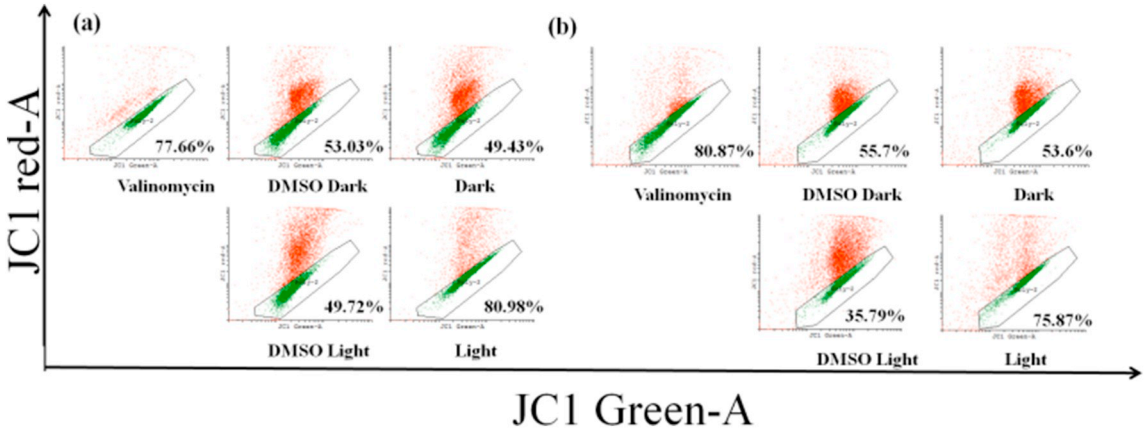


**Fig. 7.** Flow cytometric analysis (FACS) of the mitochondrial membrane potential using JC-1 (1,1′,3,3′-tetraethyl-5,5′,6,6′-tetrachloroimidacarbocyanine iodide) dye (1 μM) in (a) HeLa cells and (b) MCF-7 cells treated with complex **2** and JC-1 dye in the dark and visible light (400–700 nm). Valinomycin was used as a positive control. JC-1 permeates into the mitochondria of the cell and changes its emission from red to green as the membrane potential decreases. A significant increase in the green channel signifies altered mitochondrial function. X and Y axis of each panel represents JC1 Green-A and JC1 Red-A, respectively.

mitochondria of the cells as observed from the confocal imaging studies and mitochondrial membrane potential measurements using JC-1 assay. The nucleotide excision repair (NER) mechanism which is known to reduce the efficacy of cisplatin as nuclear DNA crosslinking agent could be circumvented by guiding the molecules to the mitochondria (mt) where circular mt-DNA is likely to be a target of the present BODIPY complexes. The diiodo-BODIPY complex **2** is unique in exemplifying dual activity in cancer biology, i.e. high PDT action in visible light with nanomolar $IC_{50}$ values in HeLa and MCF-7 cells and significant DNA crosslinking ability thus mimicking the cisplatin activity. Complex **2** with its transcription inhibition property and as a singlet oxygen generator has the potential for in vivo applications as a dual action photochemotherapeutic agent. DFT study indicated a rare cis-divacant structure of the intermediate on loss of two chloride ligands on photoexposure. This intermediate species is proposed to be mimicking the DNA crosslinking property of cisplatin.

## Abbreviations

| | |
|---|---|
| BODIPY | boron-dipyrromethene |
| ct-DNA | calf thymus DNA |
| DCFDA | 2′,7′–dichlorofluorescin diacetate |
| DMEM | Dulbecco's Modified Eagle's medium |
| DMF | dimethylformamide |
| DMSO | dimethyl sulfoxide |
| DNA | deoxyribonucleic acid |
| DPBS | Dulbecco's Phosphate-Buffered Saline |
| EB | ethidium bromide |
| FACS | fluorescence-activated cell sorting |
| FBS | fetal bovine serum |
| FITC | fluorescein isothiocyanate |
| HeLa | Henrietta Lacks |
| JC-1 | tetraethylbenzimidazolylcarbocyanine iodide |
| MCF7 | Michigan Cancer Foundation |
| MTT | 3-(4,5-dimethylthiazol-2-yl)-2,5-diphenyltetrazolium bromide |
| NC | nicked circular |
| ORTEP | Oak Ridge Thermal-Ellipsoid Plot |
| PBS | phosphate buffered saline |
| PDT | photodynamic therapy |
| PI | propidium iodide |
| ROS | reactive oxygen species |
| SC | supercoiled |
| SCE | saturated calomel electrode |
| TBAP | tetrabutylammonium perchlorate |

## Statement

This work is new. The manuscript has not been previously published, is not currently submitted for review to any other journal, and will not be submitted before a decision is made by this journal. All authors have approved the final article for submission to this journal for publication. While Arun Kumar, Somarupa Sahoo and Samya Banerjee, under my supervision, have carried out the major work with assistance from my other students Arnab Bhattacharyya, and Aditya Garai, Akanksha Dixit under the supervision of Prof. Anjali A. Karande has carried out the cellular work.

## Acknowledgements

A.R.C. thanks the Department of Science and Technology, Government of India, for financial support (SR/S5/MBD-02/2007, EMR/2015/000742) and the J.C. Bose national fellowship. A.K. and S.S. thanks Indian Institute of Science (IISc.), Bangalore, for research fellowship. A.D., S.B. and A.B. thank CSIR and University Grants Commission (UGC), New Delhi, for research fellowships. We are thankful to the Alexander von Humboldt Foundation for donation of an electrochemical system.

## Appendix A. Supplementary data

CCDC 1523110 contains the crystallographic data for complex **1**. This data can be obtained free of charge from the Cambridge Crystallographic Data Centre (CCDC) Via http://www.ccdc.cam.ac.uk/data_request/cif. Supplementary data associated with this article can be found, in the online version, at doi:https://doi.org/10.1016/j.jinorgbio.2019.110817.

## References

[1] M. Rusan, K. Li, Y. Li, C.L. Christensen, B.J. Abraham, N. Kwiatkowski, K.A. Buczkowski, B. Bockorny, T. Chen, S. Li, K. Rhee, H. Zhang, W. Chen, H. Terai, T. Tavares, A.L. Leggett, T. Li, Y. Wang, T. Zhang, T.-J. Kim, S.–.H. Hong, N. Poudel-Neupane, M. Silkes, T. Mudianto, L. Tan, T. Shimamura, M. Meyerson, A.J. Bass, H. Watanabe, N.S. Gray, R.A. Young, K.–.K. Wong, P.S. Hammerman, Cancer Discov. 8 (2018) 59–73.
[2] A. Carugo, G.F. Draetta, Cancer Discov 8 (2018) 17–19.
[3] D. Wang, B. Liu, Y. Ma, C. Wu, Q. Mou, H. Deng, R. Wang, D. Yan, C. Zhang, X. Zhu, J. Am. Chem. Soc. 139 (2017) 14021–14024.
[4] G. Karpel-Massler, C.T. Ishida, E. Bianchetti, C. Shu, R. Perez-Lorenzo, B. Horst, M. Banu, K.A. Roth, J.N. Bruce, P. Canoll, D.C. Altieri, M.D. Siegelin, Cancer Res. 77 (2017) 3513–3526.
[5] C.J. Sherr, J. Bartek, Ann. Rev. Cancer Biol. 1 (2017) 41–57.
[6] C.S. Allardyce, P.J. Dyson, Dalton Trans. 45 (2016) 3201–3209.
[7] A. Bergamo, G. Sava, Chem. Soc. Rev. 44 (2015) 8818–8835.
[8] C. Sawyers, Nature 432 (2004) 294–297.
[9] J.C. Reed, Cancer Cell 3 (2003) 17–22.
[10] N.A. Kratochwil, J.A. Parkinson, P.J. Bednarski, P.J. Sadler, Angew. Chem. Int. Ed. 38 (1999) 1460–1463.
[11] S. Havaki, A. Kotsinas, E. Chronopoulos, D. Kletsas, A. Georgakilas, V.G. Gorgoulis, Cancer Lett. 356 (2015) 43–51.
[12] E.R. Jamieson, S.J. Lippard, Chem. Rev. 99 (1999) 2467–2498.
[13] M.G. Apps, E.H.Y. Choi, N.J. Wheate, Endocr. Relat. Cancer 22 (2015) R219–R233.
[14] R. Oun, Y.E. Moussa, N.J. Wheate, Dalton Trans. 47 (2018) 6645–6653.
[15] T.C. Johnstone, K. Suntharalingam, S.J. Lippard, Chem. Rev. 5 (2016) 3436–3486.
[16] N.A. Smith, P.J. Sadler, Philos. Trans. R. Soc. A 371 (2013) 20120519.
[17] A.R. Chakravarty, M. Roy, Prog. Inorg. Chem. 57 (2012) 119–202.
[18] U. Basu, I. Khan, A. Hussain, B. Gole, P. Kondaiah, A.R. Chakravarty, Inorg. Chem. 53 (2014) 2152–2162.
[19] S. Banerjee, A. Dixit, R.N. Shridharan, A.A. Karande, A.R. Chakravarty, Chem. Commun. 50 (2014) 5590–5592.
[20] U. Basu, I. Khan, A. Hussain, P. Kondaiah, A.R. Chakravarty, Angew. Chem. Int. Ed. 51 (2012) 2658–2661.
[21] F.S. Mackay, J.A. Woods, P. Heringová, J. Kašpárková, A.M. Pizarro, S.A. Moggach, S. Parsons, V. Brabec, P.J. Sadler, Proc. Natl. Acad. Sci. U. S. A. 104 (2007) 20743–20748.
[22] Z. Liu, I. Romero-Canelón, B. Qamar, J.M. Hearn, A. Habtemariam, N.P.E. Barry, A.M. Pizarro, G.J. Clarkson, P.J. Sadler, Angew. Chem. Int. Ed. 53 (2014) 3941–3946.
[23] A.M. Evangelou, Critical Rev. Oncol. Hemato. 42 (2002) 249–265.
[24] M. Aureliano, Glob. J. Cancer Ther. 1 (2017) 12–14.
[25] W.A. Saffran, A. Ahmed, O. Binyaminov, C. Gonzalez, A. Gupta, M.A. Fajardo, D. Kishun, A. Nandram, K. Reyes, K. Scalercio, C.W. Senior, DNA Repair 21 (2014) 87–96.
[26] R. Bonnett, Chemical Aspects of Photodynamic Therapy, Gordon & Breach, London, U.K., 2000.
[27] K. Szaciłowski, W. Macyk, A. Drzewiecka-Matuszek, M. Brindell, G. Stochel, Chem. Rev. 105 (2005) 2647–2694.
[28] A.K. Renfrew, Metallomics 6 (2014) 1324–1335.
[29] S. Bonnet, Dalton Trans. 47 (2018) 10330–10343.
[30] N.J. Farrer, L. Salassa, P.J. Sadler, Dalton Trans. 28 (2009) 10690–10701.
[31] E. Alessio, Z. Guo, Eur. J. Inorg. Chem. (2017) 1539–1540.
[32] J. Piette, H.B. Gamper, A. van de Vorst, J.E. Hearst, Nucleic Acids Res. 16 (1988) 9961–9971.
[33] X. Wang, Z. Guo, Chem. Soc. Rev. 42 (2013) 202–224.
[34] S. Banerjee, A.R. Chakravarty, Acc. Chem. Res. 48 (2015) 2075–2083.
[35] S. Sahoo, S. Podder, A. Garai, S. Majumdar, N. Mukherjee, U. Basu, D. Nandi, A.R. Chakravarty, Eur. J. Inorg. Chem. (2018) 1522–1532.
[36] S. Banerjee, A. Dixit, A. Kumar, S. Mukherjee, A.A. Karande, A.R. Chakravarty, Eur. J. Inorg. Chem. (2015) 3986–3990.
[37] A. Kumar, I. Pant, A. Dixit, S. Banerjee, B. Banik, R. Saha, P. Kondaiah, A.R. Chakravarty, J. Inorg. Biochem. 17 (2017) 45–54.
[38] S.S. Soares, C. Gutiérrez-Merino, M. Aureliano, J. Inorg. Biochem. 101 (2007) 789–796.
[39] A. Kumar, A. Dixit, S. Banerjee, A. Bhattacharyya, A. Garai, A.A. Karande, A.R. Chakravarty, Med. Chem. Commun. 7 (2016) 1398–1404.
[40] D.D. Perrin, W.L.F. Armarego, D.R. Perrin, Purification of Laboratory Chemicals,

Pergamon Press, Oxford, 1980.
[41] A. Bhattacharyya, A. Dixit, K. Mitra, S. Banerjee, A.A. Karande, A.R. Chakravarty, Med. Chem. Commun. 6 (2015) 846–851.
[42] G.M. Sheldrick, SHELX–2013, Programs for Crystal Structure Solution and Refinement, University of Göttingen, Göttingen, Germany, 2013.
[43] N. Walker, D. Stuart, Acta Crystallogr. A 39 (1983) 158–166.
[44] J.L. Farrugia, J. Appl. Crystallogr. 32 (1999) 837–838.
[45] T.R. Cundari, H. Arturo, R. Leza, T. Grimes, G. Steyl, A. Waters, A.K. Wilson, Chem. Phys. Lett. 401 (2005) 58–61.
[46] M.J. Frisch, et al., GAUSSIAN 09, Gaussian Inc., Wallingford, CT, 2009.
[47] N. Adarsh, M. Shanmugasundaram, R.R. Avirah, D. Ramaiah, Chem. Eur. J. 18 (2012) 12655–12662.
[48] T.K. Goswami, B.V.S.K. Chakravarthi, M. Roy, A.A. Karande, A.R. Chakravarty, Inorg. Chem. 50 (2011) 8452–8464.
[49] (a) K. Abe, N. Matsuki, Neurosci. Res. 38 (2000) 325–329;
(b) F. Ramaekers, J. Neurosci. Methods 86 (1998) 63–69;
(c) A. Baracca, G. Sgarbi, G. Solaini, G. Lenaz, Biochim. Biophys. Acta 1606 (2003) 137–146.
[50] P. Prasad, P.K. Sasmal, I. Khan, P. Kondaiah, A.R. Chakravarty, Inorg. Chim. Acta 372 (2011) 79–87.
[51] M.C. DeRosa, R.J. Crutchley, Coord. Chem. Rev. 233-234 (2002) 351–371.
[52] G.L. Eichhorn, Y.A. Shin, J. Am. Chem. Soc. 90 (1968) 7323–7328.
[53] N. Poklar, D.S. Pilch, S.J. Lippard, E.A. Redding, S.U. Dunham, K.J. Breslauer, Proc. Natl. Acad. Sci. U. S. A. 93 (1996) 7606–7611.
[54] A.U. Khan, J. Phys. Chem. 80 (1976) 2219–2227.
[56] T. Yogo, Y. Urano, Y. Ishitsuka, F. Maniwa, T. Nagano, J. Am. Chem. Soc. 127 (2005) 12162–12163.
[57] S. Saha, D. Mallick, R. Majumdar, M. Roy, R.R. Dighe, E.D. Jemmis, A.R. Chakravarty, Inorg. Chem. 50 (2011) 2975–2987.
[58] E. Delaey, F. Van Larr, D. De Vos, A. Kamuhabwa, P. Jacobs, P. DeWitte, J. Photochem. Photobiol. B55 (2000) 27–36.
[59] A.S. Keston, R. Brandt, Anal. Biochem. 11 (1965) 1–5.
[60] N. Fozia, A. Wüstholz, R. Kinscherf, N. Metzler–Nolte, Angew. Chem. Int. Ed. 44 (2005) 2429–2432.
[61] M.W. van Gisbergen, A.M. Voets, M.H.W. Starmans, I.F.M. de Coo, R. Yadak, R.F. Hoffmann, P.C. Boutros, H.J.M. Smeets, L. Dubois, P. Lambin, Mut. Res. 764 (2015) 16–30.
[62] A. Levina, A.; P.A. P, A. Lay, Chem. Asian J 12 (2017) 1692–1699.